# Penetration Depth in Multilayered Biological Tissues using a Compact Microwave Biosensor

Joséphine Masini, Rania Shahbaz, Frédérique Deshours, Georges Alquié, Chaimae El Bastami, Hamid Kokabi

# Penetration Depth in Multilayered Biological Tissues using a Compact Microwave Biosensor

Joséphine Masini[*#1], Rania Shahbaz[*], Frédérique Deshours[*], Georges Alquié[*], Chaïmae El bastami[*], Hamid Kokabi[*]

[#]Sorbonne Université, CNRS UMR7606, Laboratoire d'Informatique de Paris 6 (LIP6), F-75005 Paris, France

[*]Sorbonne Université, CNRS, Laboratoire Génie Électrique et Électronique de Paris (GeePs), F-75005 Paris, France

[1]josephine.masini@sorbonne-universite.fr

***Abstract* — The goal of this research is to investigate microwaves penetration depth through polymorphic biological tissues. This study aims to improve an existing sensor based on a Complementary Split Ring Resonator (CSRR) structure, designed to differentiate carotid artery atherosclerotic plaques. Multilayered animal tissues (skin, fat, muscle) are studied to characterize and simulate the neck composition, where the carotid plaque is localized.**

***Keywords* — microwave propagation, biosensor, penetration testing, biological material**

## I. Introduction

Accurate properative identification of atherosclerotic plaques components is a medical challenge [1], [2]. In this objective, it is required to distinguish the composition of these plaques across the neck composed of different layers.

Since the late 1990s, scientific research has attempted to classify biological tissues via their dielectric parameters. Nonetheless, no precise method or standard has been fixed yet, particularly when characterzing multilayers of varying thicknesses in-vivo [3], [4].

Measuring the tissue's dielectric parameters and penetration depth of the electric field is especially challenging due to the scarcity of a designd and functioning measurement approach.

In previous experiments, a microwave sensor was developed for carotid plaques characterization [5], [6]. It is based on a Complementary Split Ring Resonator (CSRR) device [7] tuned to have a resonant frequency of $2.3\,\mathrm{GHz}$ when unloaded. This circular resonator is designed on a FR4 substrate ($\varepsilon_r = 4.6$, $\tan\delta = 0.028$) with an external diameter of $9.08\,\mathrm{mm}$.

This sensor is used here to determine the microwave penetration depth in various biological tissues with different thicknesses and dielectric properties. When loaded with different samples, the resonant frequency shift of the CSRR is obtained by measuring the transmission coefficient $|S_{21}(\omega)|$ and by comparing it to the unloaded measurement. This resonant frequency shift is induced by the sample's properties. Moreover, biological tissues generally present losses due to a strong microwave absorption inducing more or less attenuation of the electric field during its propagation through the sample. In addition to the composition, the thickness of each layer results in frequency variations, altering the measurement of dielectric properties [3]. As a result, the penetration depth through a multilayer structure of these tissues is extremely intricate, and the properties of a buried layer are difficult to extract.

In a first step, simulations of microwave propagation with ANSYS-HFSS and CST in only one layer will be considered (skin, fat) in order to extract dielectric parameters and penetration depth of this layer; afterwards, a multilayer with different thicknesses of these tissues will be simulated to obtain a multilayer effective model. These simulations results will be compared with experimental data obtained with the sensor by measurements done on similar animal tissues.

This study aims to indicate electric field penetration depth of this sensor when applied to the skin in order to characterise atherosclerotic plaques in the carotid artery.

## II. Method

### A. Penetration depth estimation for homogeneous materials

Before assembling and investigating the multilayer neck-model, each layer was studied respectively. The multilayer model is a stack of a skin layer followed by a layer of fat then a layer of muscle. The skin's complex structure [8] has been reduced to an epidermal layer and a layer of SAT (Subcutaneous Fat); the SAT layer is represented in Fig. 1, the dielectric constant of SAT is, in this case, more close to the fat (not infiltrated properties), because of the dryness of the samples.

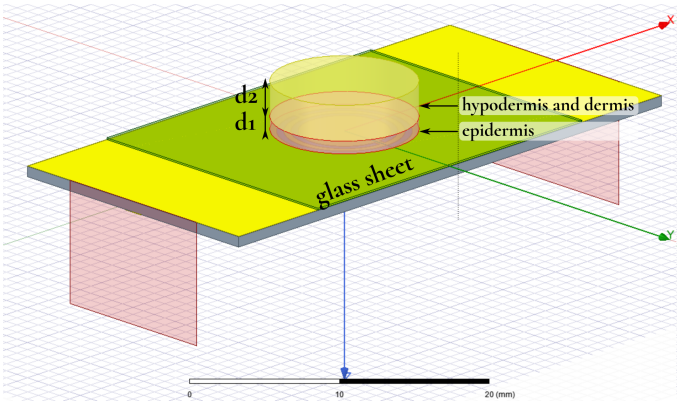


Fig. 1. Design of the simulated model

Table 1. Dielectric properties of biological tissues

| Dielectric properties | Epidermis | Dermis and hypodermis | Fat | Muscle |
|---|---|---|---|---|
| $\varepsilon'_r$ | 38.5 | 5 | 5 | 54 |
| $\tan\,\delta$ | 0.29 | 0.16 | 0.16 | 0.24 |

The penetration depth $\delta_p$ was calculated for each material, using the analytical formula (1) and the loss tangent expression (2) [9]. This formula is effective for a planar wave in a dielectric medium with losses :

$$\delta_p = \frac{1}{\frac{\omega}{c}\sqrt{\frac{\varepsilon'_r}{2}\sqrt{1+(\frac{\sigma}{\omega\varepsilon'})^2}-1}} \tag{1}$$

$$\tan\,\delta = \frac{\sigma}{\omega\varepsilon'}. \tag{2}$$

$\sigma$ is the conductivity ($\mathrm{S}\cdot\mathrm{m}^{-1}$), $\tan\,\delta$ represents losses in the tissue, $\omega$ the angular frequency ($\mathrm{rad}\cdot\mathrm{s}^{-}1$), $c = (\sqrt{\varepsilon_0\mu_0})^{-1}$ ($\mathrm{m\,s}^{-1}$) with $\varepsilon' = \varepsilon'_r\varepsilon_0$ and $\mu = \mu_0$ (no magnetic properties), $\mu_0$ and $\varepsilon_0$ are respectively vacuum's permeability and permittivity, $\varepsilon'_r$ the tissue's dielectric relative permittivity.

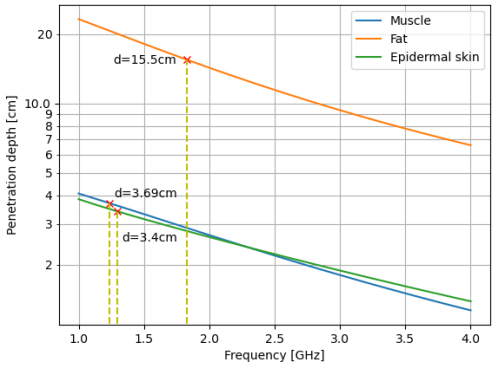


Fig. 2. Penetration depth for various biological tissues in the range 1 GHz – 4 GHz

Fig. 2 demonstrates the application of this formula for various biological tissues, showing the variation of the penetration depth in the sensor's frequency range. The values of $\varepsilon_r$ and $\tan\,\delta$ are extracted from the IT'IS virtual population database [10].

These values are indicative, as they do not consider the sensor's type, and are calculated for far-field situations.

In order to evaluate the penetration depth for each layer, a simulation model reproducing the experimental setup and shown in Fig. 1 was built using Ansys' HFSS software. The simulation model allows an easier estimation of the penetration depth, as the geometry of the tested sample can be arbitrarily resized, and various elements can be measured, such as the electric field around the sensor. For a single homogeneous layer, we consider that the maximum penetration depth is reached when between two consecutive thickness changes, the variation of the resonant frequency of the transmission coefficient $|S_{21}(\omega)|$ is below 10 MHz. The same method can be applied to the $|S_{11}|$ parameter [11].

In these simulations, injected source power is fixed at 0 dBm, but doesn't influence the results on scattering parameters as the simulation is mode-based with normalized results. In an experimental situation, different power sources will be tested to assess whether this create differences in measured parameters.

This method is illustrated in Fig. 3.

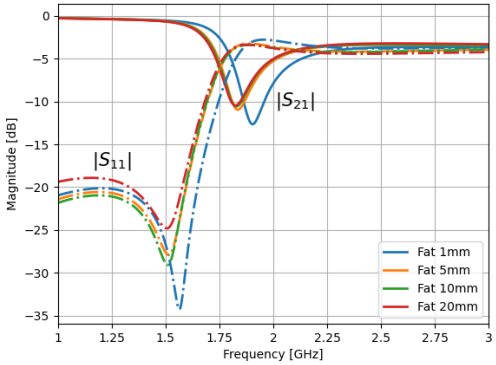


Fig. 3. Variation of the $|S_{11}|$ and $|S_{21}|$ parameters depending on the fat layer thickness

Here, the frequency shift is limited by the sensor, as $S_{21}$ and $S_{11}$ parameters are getting closer. This phenomena can be identified as the sensor's saturation, which limits the layer's thickness measurement, as the frequency shift is thus not linear and tends faster to zero as the thickness increases. Table. 2 exhibits simulated penetration depth for various tissues with the CSRR sensor.

Table 2. Sensor's penetration depth limitations

| Tissue | Resonant. freq. @ 1 mm (GHz) | Max. penetration depth $\Delta p$ (mm) | Freq. shift @ $\Delta p$ (mm) | $\lvert S_{21}\rvert_{dB}$ (dB) |
|---|---|---|---|---|
| Epidermal skin | 1.4 | 6 | 94 | −3.1 |
| Fat | 1.9 | 10 | 67 | −10.7 |
| Muscle | 1.3 | 8 | 90 | −3.1 |

### *B. Bilayer stack characterization from sensor's data*

Multilayer assessment is more complex as the sensor only provides a single set of scattering parameters, leading to a single, averaged relative permittivity $\varepsilon_{rm}$. In order to scale up to a multilayer stack of biological tissues, it is necessary to find a way to estimate each layer thickness and dielectric permittivity from global averaged values. It is possible to estimate the global relative permittivity $\varepsilon_{rm}$ for two adjacent planar layers using the relation (3) given in reference [12] for relatively thin layer thicknesses. Then a very simple two-layer model was assumed as shown in Fig. 4 :

$$\varepsilon_{rm} = \frac{\varepsilon_{r1}\cdot d_1 + \varepsilon_{r2}\cdot d_2}{d_1+d_2}. \tag{3}$$

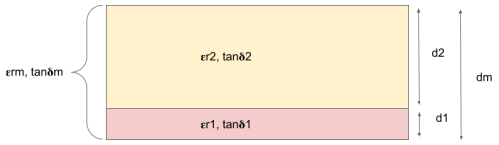


Fig. 4. Bilayer model

Before assessing this bilayer model, waves propagation through all layers must be ensured. This is done by comparing the measured transmission coefficient $|S_{21}(\omega)|$ with the one measured for the single layer samples. When the curves are identical or very close, it is hypothesized that the waves are either absorbed by the second layer or just don't pass from the first layer to the second. When the curves are different, the dielectric properties of the second layer is taken into account.

It should be then possible to extend this model to multilayer stacks in a recursive manner: the third layer can be added by considering the relative layer formed by the two firsts, and applying the formula again.

### C. Layer height and penetration depth estimation using the electric field

The formula expressed in (3) only works to uncover the stack's constitution, knowing each layer's thickness — other measures will confirm this approach. An other method has been attempted in simulation, by inspecting the electric field along the axis normal to the sensor's center, from a sufficient distance to cover the tested sample and the environmental air (at least a distance of $\lambda/2$, *i.e.* about $7\,\mathrm{cm}$ here). At the interface between two layers, microwave diffraction occurs introducing a discontinuity in the electric field (Fig. 5). The position of these peaks give an estimation of the crossed layer thickness. The precision of the interface position can depend on the difference of the permittivity of the two adjacent media.

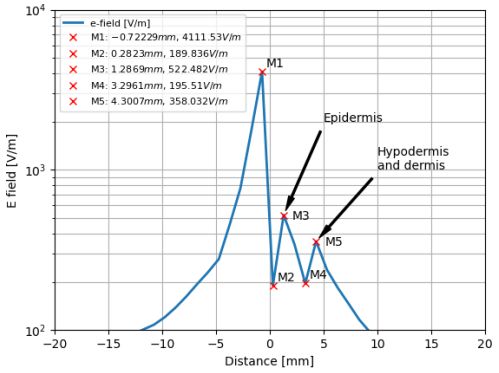


Fig. 5. Layer thickness estimation using the simulated electric field at $f = 2\,\mathrm{GHz}$

The electric field could also be used to get the penetration depth. Recalling the electric field for a planar wave with losses:

$$\mathbf{E}(z) = \mathbf{E_0} \cdot e^{\frac{-z}{\delta p}}, \tag{4}$$

for two given points if we consider $E_1 = |\mathbf{E}(z_1)|$ and $E_2 = |\mathbf{E}(z_2)|$, and by manipulating the equation (4), we can extract the penetration depth $\delta_p$:

$$\delta_p = \frac{z_2 - z_1}{\ln \frac{E_1}{E_2}}. \tag{5}$$

The formula could be applied between $M_3$ and $M_4$ to estimate the hypodermis and dermis (fat) penetration depth, after the wave propagated through the epidermis layer. Results are summarized in table Table. 3.

Table 3. Simulated penetration depth using the electric field for the bilayer model

| **Layer** | **Model thickness (mm)** | **Extracted thickness (mm)** | **Penetration depth $\delta_p$ (mm)** |
|---|---|---|---|
| Epidermis | 0.9 | 1 | N.A. |
| Hypodermis and dermis | 2.54 | 3 | 8.33 |

Measured layer thicknesses from the simulated electric field are close from the input data, with some rounding error from the layer's interface issue. The penetration depth for hypodermis and dermis layer (fat) is given at $\delta_p \approx 8.33\,\mathrm{mm}$, against $10\,\mathrm{mm}$ for the monolayer study done in Table. 2. Results are coherent as the first layer reduces the effective penetration depth for the second layer.

## III. Experimental results

### A. Skin layer

The skin layer has a $3.4\,\mathrm{mm}$ thickness and was approximated by two main layers of epidermis and fat. The epidermal layer had a dielectric constant of $\varepsilon_{r1} = 38.5$, $\tan\delta_1 = 0.29$, while the SAT layer had $\varepsilon_{r2} = 5$ to $5.3$ and $\tan\delta_2 = 0.16$.

By using (3) and by varying $d_1$, the best fit to the curve in Fig. 6 is obtained with: $d_1 = 0.9\,\mathrm{mm}$, $d_2 = 2.54\,\mathrm{mm}$, with $\varepsilon_{rm} = 14$ and $\tan\delta_m = 0.22$, which is close to the measurements in Table. 4. The epidermis represents $0.1\,\mathrm{mm}$ to $1\,\mathrm{mm}$ of the skin's constitution, and assuming the remaining composition, this evaluation gives coherent values and allows us to characterise the tested skin sample.

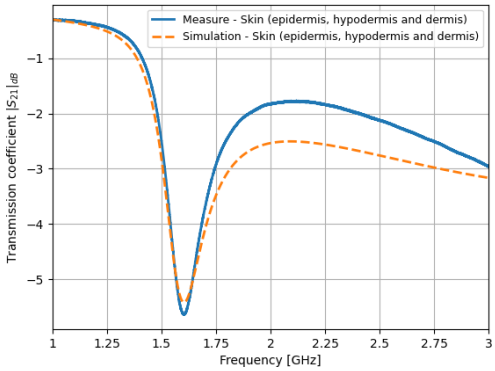


Fig. 6. Comparaison of the measured $|S_{21}|$ against simulation for a skin (epidermis, hypodermis and dermis) sample

### B. Skin and fat multilayer stack

One other measure has been made using a $1.71\,\mathrm{mm}$ thick skin sample, with a $0.9\,\mathrm{mm}$ thick epidermis and a superimposed $5.34\,\mathrm{mm}$ thick fat sample. The total thickness is $7.06\,\mathrm{mm}$. By adjusting the HFSS simulation model, the fitting curve is reached for a total thickness of $6.4\,\mathrm{mm}$, giving insights on the effective penetration depth. Results are shown on Fig. 7, and summed up in Table. 4.

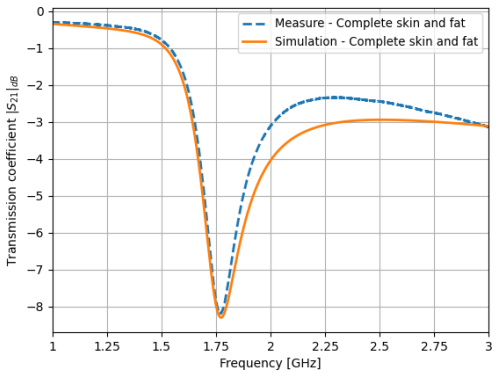


Fig. 7. Comparaison of the measured $|S_{21}|$ against simulation for a complete skin (epidermis, hypodermis and dermis) and fat sample

Table 4. Sensor's penetration depth limitations

| **Layers** | **Measured** | | **Theorical** | | **Depth** |
|---|---|---|---|---|---|
| | $\varepsilon_r$ | $\tan\,\delta$ | $\varepsilon_r$ | $\tan\,\delta$ | **(mm)** |
| Skin | 14 | 0.28 | 14.25 | 0.28 | 3.4 |
| Skin+Fat | 10 | 0.25 | 9.97 | 0.246 | 6.4 |

## IV. Conclusion

The aim of this study is to build a set of tools allowing to assess a CSRR sensor ability to see through the constitution of a multilayer biological sample. Monolayer evaluation shows that the penetration depth is limited by the sensor's saturation phenomena, which could be attenuated by lowering its resonant frequency. Multilayer characterisation is made possible by computing the equivalent permittivity of the sample, knowing its geometry. A method of unveiling the sample's geometry using the electric field gives promising results, but needs further refinement. The penetration depth could also be extracted from it, giving coherent results from the monolayer ones, and rising the fact that the penetration depth is limited by foregoing layers.

Upcoming work will be focusing on expanding the measurement database, hopefully with fresh extracted biological samples to come closer to in-vivo conditions. A muscle layer is missing to current results. A better simulation model will be created to simulate multilayer samples more accurately, as current simulation results for more than two layer samples gives incoherent results against measurements. The sensor's performance will be improved by adjusting its geometry and/or substrate to lower its resonant frequency, thus increasing its penetration depth.


## Acknowledgment

This study was done within the context of the Design and Realisation of a Miniaturized Microwwave Biosensor for a Functional Exploration of Atheromatous Biological Tissues Project.

We gratefully acknowledge the contribution of Yves Chatelon for the measurement fixture used for this study.


## References


[1] Y. Zhang, J. Cao, J. Zhou, C. Zhang, Q. Li, S. Chen, S. Feinstein, P. A. Grayburn, and P. Huang, "Plaque elasticity and intraplaque neovascularisation on carotid artery ultrasound: A comparative histological study," *European Journal of Vascular and Endovascular Surgery*, vol. 62, no. 3, pp. 358–366, Sep. 2021. [Online]. Available: https://doi.org/10.1016/j.ejvs.2021.05.026

[2] G. Goudot, J. Sitruk, A. Jimenez, P. Julia, L. Khider, J.-M. Alsac, S. E. Batti, P. Bruneval, K. Amemyia, O. Pedreira, H. Mortelette, D. Calvet, M. Tanter, T. Mirault, M. Pernot, and E. Messas, "Carotid plaque vulnerability assessed by combined shear wave elastography and ultrafast doppler compared to histology," *Translational Stroke Research*, vol. 13, no. 1, pp. 100–111, Jun. 2021. [Online]. Available: https://doi.org/10.1007/s12975-021-00920-6

[3] A. V. Vorst, A. Rosen, and Y. Kotsuka, *RF / microwave interaction with biological tissues*, ser. Wiley Series in Microwave and Optical Engineering. New York, NY: Wiley-IEEE Press, Feb. 2006.

[4] A. L. Gioia, E. Porter, I. Merunka, A. Shahzad, S. Salahuddin, M. Jones, and M. O'Halloran, "Open-ended coaxial probe technique for dielectric measurement of biological tissues: Challenges and common practices," *Diagnostics*, vol. 8, no. 2, p. 40, Jun. 2018. [Online]. Available: https://doi.org/10.3390/diagnostics8020040

[5] R. Shahbaz, F. Deshours, G. Alquie, H. Kokabi, F. Koskas, I. Brocheriou, G. Lenaour, C. Hannachi, and J.-M. Davaine, "Diagnosis of atheromatous carotid plaque: Dielectric constant measurement using microwave resonant technique versus ultrasound b-mode images," in *2021 USNC-URSI Radio Science Meeting (USCN-URSI RSM)*. IEEE, Aug. 2021. [Online]. Available: https://doi.org/10.23919/usnc-ursirsm52661.2021.9552356

[6] F. Deshours, G. Alquié, G. Tawous, H. Kokabi, J.-M. Davaine, and F. Koskas, "Modélisation de résonateurs en anneaux fendus pour la mesure de permittivités complexes," in *XXIèmes Journées Nationales Microondes*, 2019.

[7] J. Baena, J. Bonache, F. Martin, R. Sillero, F. Falcone, T. Lopetegi, M. Laso, J. Garcia-Garcia, I. Gil, M. Portillo, and M. Sorolla, "Equivalent-circuit models for split-ring resonators and complementary split-ring resonators coupled to planar transmission lines," *IEEE Transactions on Microwave Theory and Techniques*, vol. 53, no. 4, pp. 1451–1461, Apr. 2005. [Online]. Available: https://doi.org/10.1109/tmtt.2005.845211

[8] Anatomy of the skin. [Online]. Available: https://www.stanfordchildrens.org/en/topic/default?id=anatomy-of-the-skin-85-P01336

[9] S. W. Ellingson. (2020, may 9) Loss Tangent. [Online]. Available: https://phys.libretexts.org/@go/page/24785

[10] P. Hasgall, F. Di Gennaro, C. Baumgartner, E. Neufeld, B. Lloyd, M. Gosselin, D. Payne, A. Klingenböck, and N. Kuster. (2022, Feb 22) It'is database for thermal and electromagnetic parameters of biological tissues. [Online]. Available: https://itis.swiss/virtual-population/tissue-properties/overview/

[11] M. Calvet-Chautard, "Instrumentation radiofréquence pour l'agriculture de précision : application à la filière aviaire pour le suivi non-invasif du poids de foie," Ph.D. dissertation, Univ. Toulouse 3, Toulouse, 2020. [Online]. Available: http://www.theses.fr/2020TOU30147

[12] R. Dib, "Caractérisation de couches diélectriques et magnétiques de structures multicouches par cavité résonante microonde," Theses, Université Jean Monnet - Saint-Etienne ; Université Libanaise, Oct. 2014. [Online]. Available: https://tel.archives-ouvertes.fr/tel-01187109